Moutet *et al. Energy Mater* 2024;4:400024
DOI: 10.20517/energymater.2023.92

Energy Materials

Article

Open Access

Check for updates

Designing the next generation of symmetrical organic redox flow batteries using helical carbocations

Jules Moutet, Tarek H. El-Assaad, Ramandeep Kaur, David D. Mills, Thomas L. Gianetti*

Department of Chemistry and Biochemistry, University of Arizona, Tucson, AZ 85719, USA.

***Correspondence to:** Prof. Thomas L. Gianetti, Department of Chemistry and Biochemistry, University of Arizona, 1306 E. University Blvd., Tucson, AZ 85719, USA. E-mail: tgianetti@arizona.edu

How to cite this article: Moutet J, El-Assaad TH, Kaur R, Mills DD, Gianetti TL. Designing the next generation of symmetrical organic redox flow batteries using helical carbocations. *Energy Mater* 2024;4:400024. https://dx.doi.org/10.20517/energymater.2023.92

Received: 8 Nov 2023 **First Decision:** 21 Dec 2023 **Revised:** 8 Jan 2024 **Accepted:** 4 Mar 2024 **Published:** 20 Mar 2024

Academic Editors: Yizhong Huang, Cristina Flox Donoso **Copy Editor:** Fangling Lan **Production Editor:** Fangling Lan

Abstract

In recent years, non-aqueous fully organic Redox Flow Batteries (RFBs) have displayed potential in broadening the electrochemical window and enhancing energy density in RFBs by relying on redox-active organic molecules to provide improved sustainability in comparison to metal-based charge carriers. Of particular interest, systems that rely on a single bipolar redox molecule (BRM) for their operation, known as symmetrical organic RFBs, have gained momentum as the utilization of a BRM eliminates membrane crossover issues, thus extending the lifespan of electrical energy storage systems while reducing their cost. In this manuscript, we will present our contribution to this field through the design of tunable bipolar molecules within the helicene carbocation class. This particular type of BRM is synthetically very affordable and has proven to be highly modifiable and robust. Through the examination of 11 examples, we will demonstrate how an approach based on readily available electrochemical tools can be efficiently employed to generate and assess a library of compounds for future full flow RFB applications.

Keywords: Electrochemistry, energy storage, symmetric organic redox flow battery, carbenium ion, electrolyte design, helicenium

INTRODUCTION

Meeting the ever-growing global energy demand is an urgent imperative, necessitating the development of

energy-storage solutions. These solutions play a crucial role in facilitating the transition to renewable energy grid integration, decarbonizing our economy, and tackling the challenges posed by global warming[1-3]. In order to achieve the objectives outlined in the International Energy Agency roadmap[4], the emergence of a variety of metal-based battery solutions has been observed[5-8], notably marked by the widespread adoption of high-performance lithium-ion batteries[9-11]. However, as concerns about fire hazards linked to the accumulation of low-valent metal have risen and the current demand rapidly overtaking the availability of this metal[12,13], the industry is being directed toward safer, cost-effective, and scalable electricity energy storage (EES) solutions[14,15]. Redox flow batteries (RFBs) have emerged as a compelling choice for large-scale stationary applications within the EES domain, primarily because of their engineering adaptability and scalability enabled by the decoupling of power and capacity[16-19].

Currently, commercially established RFB technologies are based on the redox characteristics of transition metal ions in aqueous solutions (AqRFBs). Among these, the most extensively studied options are vanadium oxide and chromium and iron variants[20-24]. Nevertheless, several drawbacks hinder the widespread deployment of AqRFBs, such as the limited electrochemical stability window of water (1.5 V), low energy densities induced, high costs associated with ionic separators, environmental implications related to ore mining, management of substantial quantities of acid, and the inherent toxicity of certain compounds[25-27].To broaden the electrochemical window and enhance energy density under mild pH conditions, non-aqueous RFBs present a significant advancement[28-30]. They enable the use of Redox-active Organic Molecules (ROMs), demonstrating enhanced sustainability compared to transition metal-based redox-active materials[31]. ROMs have a lower global warming potential index, indicating an environmental impact one-fourth that of transition metal-based materials[32]. Moreover, they will ensure a consistent market price at one-fourth the cost per kilogram and can be sustainably sourced and tailored synthetically[31-33]. Most of reported Non-Aqueous fully-Organic RFBs (NAORFBs) exhibit an asymmetric configuration, using two distinct ROMs as catholyte and anolyte. This setup imposes selectivity requirements on the exchange membrane, leading to alternative avenues for chemical degradation and irreversible capacity fading[34,35]. Various effective approaches have been investigated to mitigate redox-active material crossover, including interface improved size selectivity[36,37], enhanced membrane composition[38-40], and eliminating the need for a membrane by adopting tandems of non-miscible redox electrolytes[41].

Concurrently, with the rise of innovation in the field, an elegant solution has emerged: drawing inspiration from vanadium RFBs (VRFBs) and their quasi-identical tank chemistry, symmetrical Organic RFBs (SORFBs) have gained prominence as the most promising approach for eliminating membrane crossover and prolonging EES lifespan[23,42-44]. The primary characteristic of SORFBs lies in their use of a singular bipolar redox molecule (BRM) on both sides of the cell[45]. This robust molecule features in its initial state - at least- three stable redox states, owing to entirely reversible reduction and oxidation processes. Consequently, these molecules can function as both anolyte and catholyte within a battery[46-48]. The resultant symmetrical RFB relies on identical solution components in each half-cell, offering notable advantages[42]. Firstly, using the same redox-active material reduces the chemical gradient of electroactive species, negating the necessity for highly selective membranes and effectively mitigating crossover. In the event of crossover, rather than enduring permanent contamination, SORFBs will undergo self-discharge[23]. Furthermore, when in the discharged state, there is no chemical or electrochemical gradient across the membrane, guaranteeing SORFBs to be stored indefinitely without contamination due to leakage or irreversible side reactions. Finally, recent research has demonstrated that capacity loss resulting from compound degradation can be reclaimed through regular polarity reversals, thus extending the battery lifespan[42,49-51]. Additionally, relying on a single charge carrier species could help achieve significant economies of scale while streamlining the supply chain for broad implementation. The recent surge in

SORFB progress has inspired chemists to craft a varied array of BRMs, employing three molecular approaches to fashion novel redox-active compounds [Figure 1][45].

Redox-active organic materials are usually categorized as *n*-type or *p*-type based on their ability to either store or provide electrons in their neutral state during electrochemical reactions. *n*-type redox-active organic materials typically experience reduction from their neutral state, resulting in a negatively charged molecular state. In contrast, *p*-type organic materials undergo oxidation from their neutral state, yielding positively charged. Both ROMs must exhibit reversible redox events to be used. One straightforward method involves pairing an *n*-type moiety with a *p*-type moiety using a simple linker, most of the time insulating [Figure 1A]. The resulting molecule can function as a bipolar entity ($^{-\bullet}n$-$p \rightleftharpoons n$-$p \rightleftharpoons n$-$p^{\bullet+}$), provided that none of its three redox states are compromised or interact with uncharged molecules in the medium. This "combi-molecule" approach[65] is both fundamental and effective, as it leverages the extensive research conducted on catholyte and anolyte structures for fully organic RFBs, each with a known potential, leading to a BRM with a predicted potential gap ($E_{gap} = E_{1/2}^{Ox} - E_{1/2}^{Red}$) between both sides of the SORFB[43,52-58]. However, this approach underutilizes half the molecule on each battery side, reducing atom efficiency and significantly increasing the molecular weight of the charge carrier, limiting potential energy density per kilogram of ROM[66].

An improved strategy for developing innovative BRMs enhances this design concept by electronically merging established *n*-type and *p*-type conjugated scaffolds within a single molecule [Figure 1B]. By closely integrating the conjugation of two aromatic materials, the electronic characteristics of each component are anticipated to synergistically influence the resulting electrochemical potentials. Rising the E_{gap} while maintaining a reasonable molecular weight ensures a favorable capacity per unit weight. This route has proved successful, leading to the formation of closed-shell[49,58,60,67] and open-shell molecules[59,68] that exhibit improved properties compared to their parent units. Nonetheless, the synthetic access to such compounds can be a gradual and intricate process, involving multiple steps and introducing the risk of antagonism effects due to significant structural alteration of the initial *n*- and *p*- moieties. And, in contrast to method a, only a comprehensive electrochemical assessment of the final molecule can guarantee stability across all oxidation states ($^{-\bullet}n|p \rightleftharpoons n|p \rightleftharpoons n|p^{\bullet+}$).

The latest approach shifts away from merging the electronic characteristics of *n*- or *p*-type molecules. Instead, it revolves around exploring existing literature for compounds that exhibit bipolar activity (Figure 1, $^{-\bullet}$Ab $\rightleftharpoons$ Ab $\rightleftharpoons$ Ab$^{\bullet+}$). Although such compounds are relatively scarce, the concept of relying on already well-defined and robust bipolar molecules proves refined and straightforward. Consequently, this facilitates maintaining a low molecular weight while customizing the scaffold to enhance E_{gap}, stability, solubility, or cost-effectiveness [Figure 1C]. Along this path, open-shell compounds, acting as ambiphilic radicals with three stable states, have achieved significant success when appropriately managing their inherent reactivity[51,61,62,69]. The search for additional ambipolar compounds can be rooted in redox-active ligands featuring multiple stable states commonly found in homogeneous catalysis[63,64,70] or in organophotocatalysis characterized by three well-defined redox states[71].

Aligned with strategy (c) and contributing to the SORFB research field, our group chose to employ a specific category of BRMs within the carbenium ion class. Among the members of this carbocation family, certain compounds have demonstrated exceptional stability[72-74] and hold significant utility in coordination chemistry[75-77], small molecules activation[78,79], and, notably, organophotocatalysis[80-86]. And while a planar triangulenium motif has recently enabled the deployment of a robust SORFB model[87], it is the particularly rich and versatile chemistry of [4]helicenium ions that will be discussed in what follows[88].

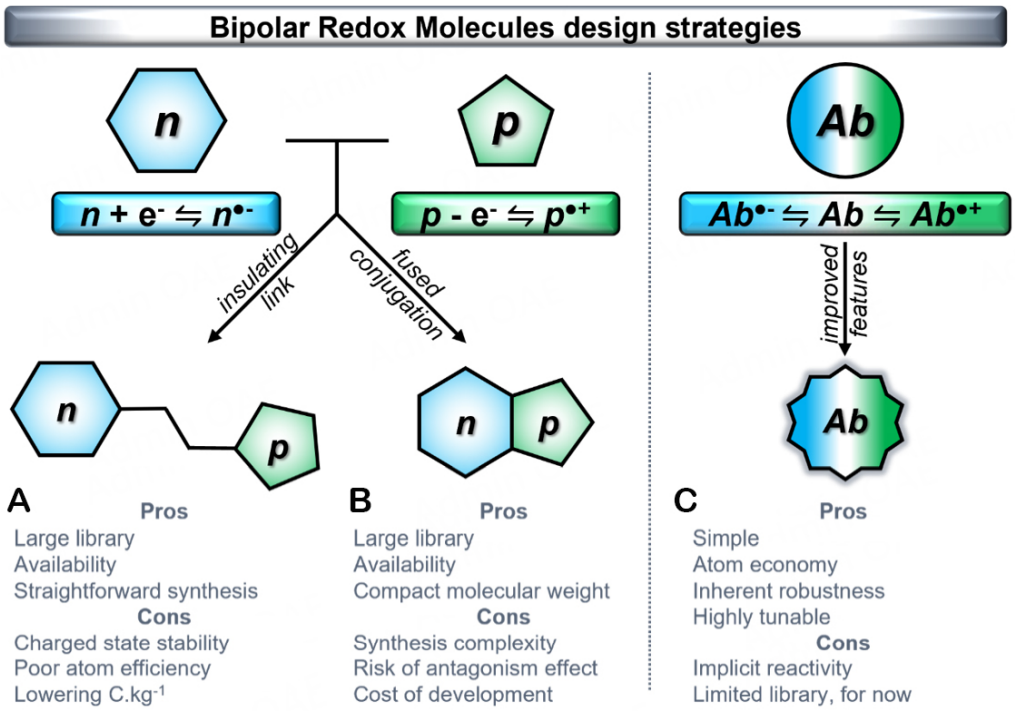

Figure 1. Three strategies to develop innovative bipolar redox molecules for the rise of Symmetrical Organic Redox Flow Battery. *n* corresponds to *n*-type molecules, *p* for *p*-type molecules, while *Ab* means for ambiphilic molecules. Examples of SORFBs based on strategy (A) could be found in the references[52-58], strategy (B) at[49,50,59,60] and strategy (C) at[51,61-64].

Dimethoxyquinacridiniums ($DMQA^+$) are sturdy helical carbenium ions, well-documented for their biological applications, photophysical features and electrochemical properties[89-96]. The reversible electrochemical oxidation and reduction processes involving these carbenium ions have been notably disclosed by Herse and Sørensen *et al.*[89,97]. In line with this, our group has recently published a study on the chemical synthesis, isolation, and characterization of neutral helicene radicals produced through chemical reduction of the corresponding carbocation precursors[98]. All of these preliminary efforts have enabled us to introduce a robust SORFB model based on a relatively straightforward *N,N′*-di-*n*-propyl-1,13-dimethoxyquinacridinium ($^{nPr}DMQA^+$) with the capability to operate in a poleless mode[99]. This research led to the publication of a second model featuring an enhanced $DMQA^+$ framework through nitro group incorporation ($^{nPr}DMQA^{NO2+}$), resulting in a significant boost in energy density at the expense of stability[100].

In this context, this work aims to demonstrate how the utilization of pre-established bipolar redox scaffolds facilitates effective screening. We propose a methodology for rapidly evaluating the properties and compatibility of new BRMs for SORFB deployment. This approach is illustrated through the examination of 11 differently substituted helicenium examples, leveraging our expertise on the $DMQA^+$ core. The results will be showcased through electrochemical characterization using a three-electrode cell. A thorough investigation of electrochemical kinetic parameters will help qualify the effects induced by various substitutions and structure tethering. Lastly, the robustness of ROMs, which have demonstrated suitable parameters for use in the RFB field, will be evaluated through cycling in H-cells, also known as “static RFB”.

EXPERIMENTAL

General remarks

All solvents were purified by solvent purification system (SPS) or distillation over the drying agents indicated. Dried solvents and liquid reagents were transferred by oven-dried or hypodermic syringes. The supporting electrolyte salts, tetrabutylammonium hexafluorophosphate ($TBAPF_6$) and tetrabutylammonium tetrafluoroborate ($TBABF_4$), were recrystallized three times from ethanol and then dried at 80 °C for three days prior to use in the glovebox. All glassware or hardware has been dried in an oven at least 24 h prior to introduction in a glovebox.

Details of helicenium compound synthesis and nomenclature are available in Supplementary Table 1 and Supplementary Materials Synthesis part.

Electrochemistry

Electrochemical analyses were conducted inside an Argon-filled MBraun Unilab glovebox using a BioLogic SP-200 potentiostat/galvanostat and the EC-Lab® software (v11.50) from BioLogic Science Instruments. For convenience, potentials are expressed versus internal reference electrode $AgNO_3$/Ag (E_{ref}, 0.01 M $AgNO_3$ in 0.1 M $TBAPF_6$ in CH_3CN).

Cyclic voltammetry and electrokinetic parameters determination

Cyclic voltammograms (CV) were obtained in a three-electrode electrochemical cell, which included a counter electrode (E_c) made of platinum wire, an $AgNO_3$/Ag reference electrode (E_{ref}), and a working electrode (E_w, 0.071 cm^{-2}, CH Instrument, Inc.) composed of glassy carbon. Prior to each measurement, the working electrode was meticulously polished using aluminum oxide on polishing paper and anhydrous CH_3CN to eliminate any remaining particles. Unless stated otherwise, all measurements have been recorded for 1 mM of BRM in a 0.1 M $TBAPF_6$ CH_3CN solution. To determine the diffusion and electron transfer rate coefficient, CVs of each electronic process have been recorded at various scan rates: 10, 25, 75, 100, 250, 400, and 500 $mV{\cdot}s^{-1}$.

Static RFB cycling

Bulk charge/discharge cycling was conducted within a homemade H-cell, where a porous glass frit served as the separator[101,102]. Reticulated vitreous carbon (RVC) electrodes were utilized as E_w and E_c, cut into standardized dimensions, and then disposed of at the conclusion of each experiment to eliminate the possibility of contamination. A Constant Current |5 mA| followed by a Constant Voltage Galvanostatic Charging with Potential Limitation (CCCV GCPL protocol) was applied via the RVC electrodes. Both chambers of the H-cell were filled with 5 mL of electrolyte/ROM and were continuously agitated with magnetic stir bars at 1,000 rpm. An equilibration period of two hours was observed prior to active charging and discharging. Details and dimensions are available in Supplementary Materials.

RESULTS AND DISCUSSION

The choice of the [4]helicenium motif as the core for structural modifications is related to its high durability and the numerous applications we have attributed to it within our research group. Indeed, the $DMQA^+$ core, a stable carbocation in both air and water in its synthesized form, exhibits three stable redox states. The $DMQA^+$ can thus be electrochemically reduced by one electron to form a neutral $DMQA^{\bullet}$ radical at $E_{1/2}^{Red}$ and conversely oxidized by one electron to form a $DMQA^{\bullet++}$ dication radical at $E_{1/2}^{Ox}$ [Figure 2].

The access and stability of these two states are crucial for obtaining a suitable BRM for symmetrical RFBs. Hence, all structural modifications explored must be compatible with the various oxidation states. Two

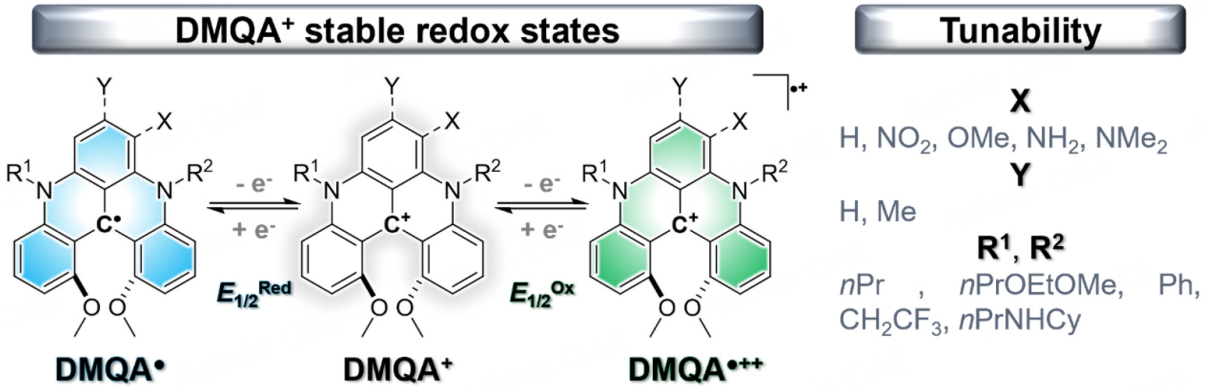

Figure 2. Stables redox states of DMQA$^+$ core and structural modifications explored in this study.

variation types that showcase the extensive tunability of the DMQA$^+$ motif can be investigated. Alterations of the aromatic core of the DMQA$^+$ motif through positions X or Y with electrophilic or nucleophilic groups are feasible and detailed at various synthesis stages, whether initially on the tris-aryl carbenium synthon for Y or during the late functionalization stage for X [Supplementary Figure 1][94,100]. Changes in the nature of the R^1 and R^2 "arms" are almost invariably introduced during a double nucleophilic aromatic substitution [Supplementary Figure 1][103].

Considering the results obtained with the SORFB model based on ^{nPr}DMQA$^+$[99], initially, we examined the consequences of modifying the X group through late-stage functionalization. The synthesis of these compounds had been well described and was achievable by adding only a few steps to the initial synthesis path[94]. The groups NO_2, OMe, NH_2, and NMe_2, along with their influence on the electrochemical properties of the ^{nPr}DMQA$^+$ scaffold as a reference, were thus studied in acetonitrile, our model solvent (Figure 3, ^{nPr}DMQA$^+$ as black trace)[104,105]. The impact of the X-position substitution on the core has proved to be significant for the E_{gap} and, thus, for attainable energy density[31]. As previously reported, the introduction of an electron-attracting nitro group contributes to shifting the potentials of the $E_{1/2}^{Red}$ and $E_{1/2}^{Ox}$ processes towards the cathodic region of the spectrum, while introducing a second reversible reductive event (Figure 3 red trace). In addition, the gap between these fully reversible processes was increasing, transitioning from E_{gap} = 2.12 V to E_{gap} = 2.24 V[100]. Conversely, when an OMe ether group is added at the X position, a slight decrease in the $E_{1/2}^{Red}$ potential (-60 mV) is observed, while the $E_{1/2}^{Ox}$ value drops by 220 mV, resulting in a lower E_{gap} of 1.84 V (Figure 3 orange trace). Following this trend, the introduction of a primary amine NH_2 and a tertiary NMe_2 at the X position only minimally affects the value of the DMQA$^+$ core reduction process, with a maximum difference of -20 mV for $E_{1/2}^{Red}$ compared to ^{nPr}DMQA$^+$. However, a drastic decrease in the value of $E_{1/2}^{Ox}$ is noted in both cases, with a value of -510 mV for ^{nPr}DMQA^{NH2+} and -560 mV for ^{nPr}DMQA^{NMe2+}, leading to E_{gap} values of 1.60 and 1.54 V, respectively (Figure 3 yellow and salmon traces).

When it comes to modifying the Y position of the aromatic core, options for late-stage functionalization are practically absent. The alteration of this position in the para of the carbocation center of tris-aryl carbenium synthons must take place during a preliminary step [Supplementary Figure 1]. Access to an electronically enriched scaffold through the introduction of OMe and NMe_2 groups was unsuccessful[72,106]. Despite numerous attempts, the electron richness of acridinium moieties containing three σ- and π-donating groups, such as OMe and NMe_2, in the para position inhibits the second aromatic nucleophilic substitution required to form the helicenium scaffold[83]. Fortunately, σ-donating groups such as methyl groups which were introduced in the para position to form the synthon tris(2,6-dimethoxy-4-methylphenyl)carbenium

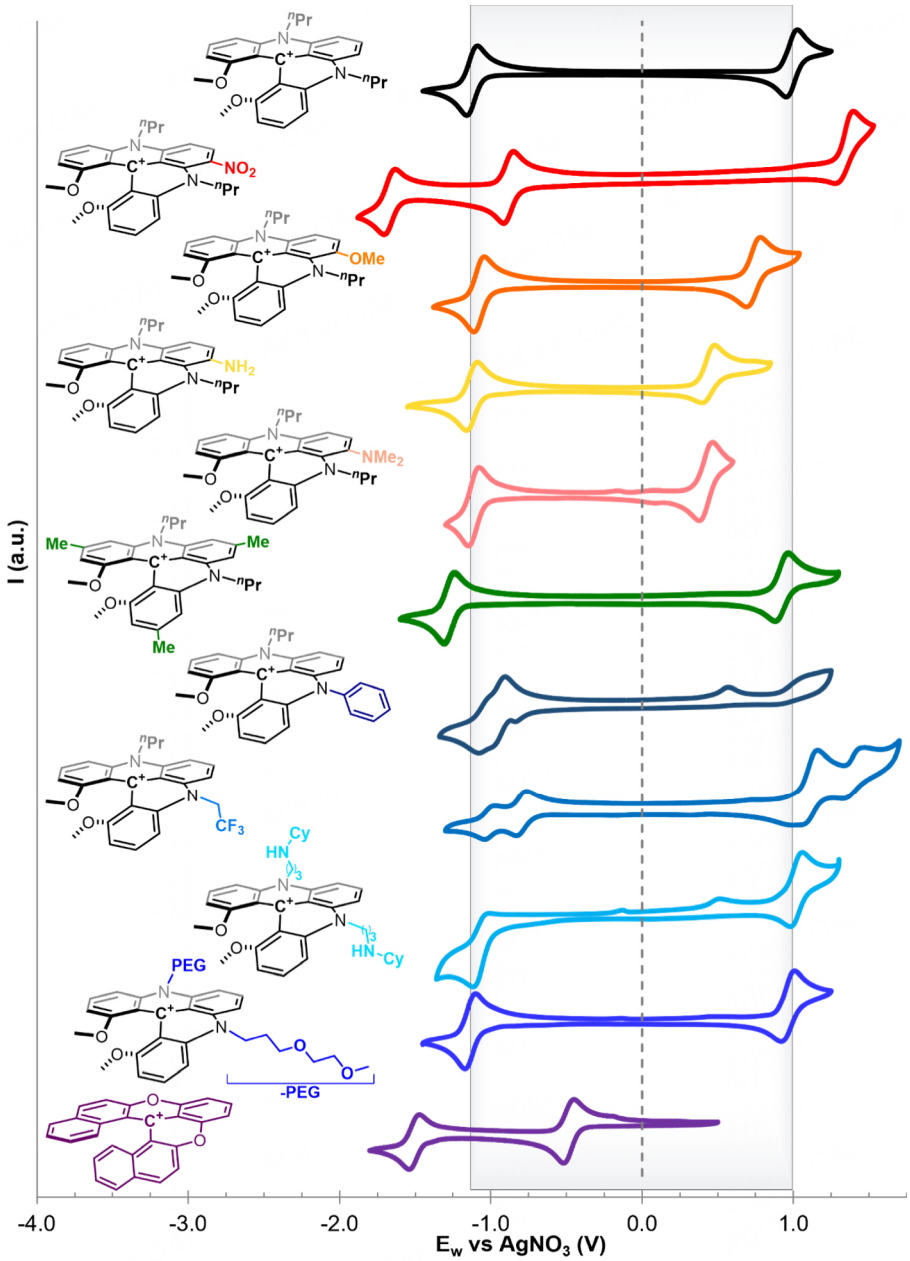

Figure 3. Cyclic voltammograms of 1 mM ^{nPr}DMQA$^+$, ^{nPr}DMQA^{NO2+}, ^{nPr}DMQA^{OMe+}, ^{nPr}DMQA^{NH2+}, ^{nPr}DMQA^{NMe2+}, ^{nPr}DMQA$^{(pMe)3+}$, $^{nPr/Ph}$DMQA$^+$, $^{nPr/CH2CF3}$DMQA$^+$, $^{(CyNHnPr)}$DMQA$^+$, ^{PEG}DMQA$^+$ and [6]helicene$^+$ in 0.1 M $TBAPF_6$ CH_3CN solution at 100 mV·s^{-1}. All values of potential are reported in Table 1. Grey box corresponding to E_{gap} of ^{nPr}DMQA$^+$.

tetrafluoroborate did not hamper the synthesis of the helicenium analog DMQA$^{(pMe3)+}$ (see Supplementary Materials). This new compound sees its $E_{1/2}^{Red}$ value decrease by -130 mV, while its $E_{1/2}^{Ox}$ value only decreases by -60 mV compared to ^{nPr}DMQA$^+$. This leads to an E_{gap} = 2.19 V, which is significantly comparable to the reference DMQA$^+$ (Figure 3 green trace).

We then focus our interest on the nature of the arms carried by the DMQA$^+$ scaffold and their impact on the electrochemical properties of the BRM. Through the introduction of a Ph group in R^2 through a preliminary synthesis step, followed by adding an *n*Pr group in R^1, a dissymmetrical DMQA$^+$ was

obtained[103]. It was quickly observed that the presence of a Ph aromatic group, while not significantly altering the potential of the electrochemical events, severely disrupts their reversibility (Figure 3 deep blue trace). The $E_{1/2}^{Red}$ was recorded at -0.99 V *vs*. $AgNO_3$, a difference of +150 mV compared to the ^{nPr}DMQA$^+$, while the E^{Ox} became completely irreversible. This initial drawback renders this molecule unsuitable for the deployment in SORFB. The substitution of the R^2 arm with an electrophilic trifluoroalkyl group CH_2CF_3 was then initiated to assess its influence on the electrochemical processes (Figure 3 sky blue trace). It was observed that the $E_{1/2}^{Red}$ potential shifted towards more positive values by +340 mV, with the appearance of a second distinct process $E_{1/2}^{Red2}$. The $E_{1/2}^{Ox}$ process was measured higher by +110 mV as compared to the reference DMQA$^+$ but also became bielectronic, making use of $^{nPr/CF_3CH_2}$DMQA$^+$ as a BRM very complicated as the electron exchanges would be unbalanced. From a more structural perspective rather than electronic, the introduction of two bulky amino-alkyl R^1/R^2 arms (3-(cyclohexylamino)propyl) in order to increase the molecule's steric hindrance does not seem to induce any noticeable effect on the E^{Red} and E^{Ox} processes, which are modified by +160 and +50 mV, respectively (Figure 3 light blue trace). However, this $^{(CyNHnPr)}$DMQA$^+$ molecule experiences an alteration of both processes as they became pseudo-reversible. The pursuit of increased solubility of the different oxidation states of the DMQA$^+$ core has also guided the synthesis of a variation where R^1 and R^2 were introduced in the form of an alkyl ether moiety, so-called pegyl chain (3-(2-methoxyethoxy)propyl = PEG)[45,107]. Remarkably, this ^{PEG}DMQA$^+$ molecule presents values of $E_{1/2}^{Red}$ and $E_{1/2}^{Ox}$ very similar to those of the reference ^{nPr}DMQA$^+$, with potential variations less than -50 mV, allowing the preservation of an E_{gap} = 2.07 V (Figure 3 blue trace)[108].

Finally, the rich chemistry of heliceniums[109] prompted us to take an interest in dioxo[6]helicenium (labeled [6]helicene$^+$ in Figure 3 and Table 1). [6]helicene$^+$ is a parent helicenium of diaza[4]helicenium, the DMQAs presented thus far, devoid of R^1/R^2 arms where the bridging amino groups (NR) are replaced by a bridging oxygen atom. Expansion from [4] to [6]helicenes is provided by replacing the methoxy groups of the core with phenyl rings[110]. This [6]helicene$^+$ presents two completely reversible reduction phenomena with a first reduction at $E_{1/2}^{Red}$ = -0.48 V *vs*. $AgNO_3$ at a much higher potential than the reduction of the DMQA$^+$ model consistent with the less electron donating effect of the O *vs*. NR bridge groups (Figure 3 purple trace). However, no reversible electrochemical process is accessible in oxidation, consequently eliminating this molecule, as well as $^{nPr/Ph}$DMQA$^+$, from use as a BRM, and these heliceniums will not be further discussed hereafter.

While the development of new BRMs for the deployment of SORFB is experiencing significant growth, it should be noted that a certain lack of coherence in the reporting and evaluation methods of their physicochemical specificities makes the comparison of new ROMs difficult[111]. However, certain kinetic parameters need to be highlighted. Thus, parameters such as diffusion (D) and electron-transfer rate (k^0) will greatly determine the expected performances for using a ROM in SORFB. Through effective mass transport of the different oxidation states of the BRM from the bulk solution to the electrode surface, higher current density can be achieved while limiting overpotential. The importance of the parameter k^0 lies in its description of the efficiency of electron transfer from the electrodes to the ROM. Its value range also indicates the reversibility of the electronic process, with complete reversibility above 10^{-1} cm·s^{-1}, quasi-reversibility between 10^{-1} and 10^{-5} cm·s^{-1}, and irreversibility below this range[112]. While having the highest possible values of D and k^0 is indeed preferable, it should be noted that in the context of BRMs and due to the symmetrical aspect of SORFBs and the use of a single molecule, it is also important that the values corresponding to the reduction and oxidation processes are in the same order of magnitude. This is to avoid any overpotential or loss of energy efficiency due to significant differences in kinetics during full flow deployment.

Table 1. Summary of $E_{1/2}^{Red/Ox}$, E_{gap}, diffusion parameters (D) and electron-transfer rate parameters (k^0) of 1 mM $^{R1/R2}DMQA^{X/Y+}$ measured in 0.1 M $TBAPF_6$ CH_3CN. All potentials are expressed against $AgNO_3$/Ag. Sets of 7 scan rates for electronic processes of each helicenium are available in Supplementary Figures 2-8.

Compound	$E_{1/2}^{Red}$ (V)	$E_{1/2}^{Ox}$ (V)	E_{Gap} (V)	D (×10^{-6} cm^2/s)		k^0 (×10^{-2} cm/s)	
				$E_{1/2}^{Red}$	$E_{1/2}^{Ox}$	$E_{1/2}^{Red}$	$E_{1/2}^{Ox}$
$^{nPr}DMQA^+$	-1.14	0.98	2.12	9.49	9.99	2.65	2.04
$^{nPr}DMQA^{NO2+}$	-0.89	1.35	2.24	5.57	9.87	3.69	0.79
$^{nPr}DMQA^{OMe+}$	-1.08	0.76	1.84	5.27	5.03	2.50	1.01
$^{nPr}DMQA^{NH2+}$	-1.13	0.47	1.60	10.1	9.62	2.48	0.96
$^{nPr}DMQA^{NMe2+}$	-1.12	0.42	1.54	5.70	4.05	2.23	0.66
$^{nPr}DMQA^{(pMe)3+}$	-1.27	0.92	2.19	5.82	4.12	3.43	0.293
$^{nPr/Ph}DMQA^+$	-0.99	*irr*	-	4.01	*irr*	0.15	*irr*
$^{nPr/CH2CF3}DMQA^+$	-0.80	1.09*	1.89*	0.78	3.86	1.64	0.12
$^{(CyNHnPr)}DMQA^+$	-0.98‡	1.03‡	2.01	5.87	4.03	0.50	1.11
$^{PEG}DMQA^{+\dagger}$	-1.13	0.94	2.07	6.24	6.24	24.5	1.13
[6]helicene$^+$	-0.48	*irr*	-	8.63	*irr*	2.45	*irr*

*$2e^-$ process, imbalanced for a SORFB; †recorded in CH_3CN 0.5M $TBABF_4$; ‡pseudo-reversible.

During the study of the reversibility of the electronic processes of each helicene, in-depth studies of the electrokinetic parameters D and k^0 of each of them were conducted for practical reasons under the conditions of cyclic voltammetry. For this purpose, CVs of isolated electronic events were performed at seven different scan rates (10, 25, 75, 100, 250, 400, and 500 mV·s^{-1}). D determination was relying on the resolution of the Randles-Sevcik equations [Supplementary Equation 1] and k^0 on the numerical application of the method developed by Nicholson *et al.* and Lavagnini *et al.* [Supplementary Equation 2][113,114].

The preliminary studies and results conducted on compounds $^{nPr}DMQA^+$ and $^{nPr}DMQA^{NO2+}$ have already demonstrated good performances in static RFBs. Indeed, the reference carbenium with diffusion coefficients close to 1 × 10^{-5} cm^{-2}·s^{-1} and k^0 at 2 × 10^{-2} cm·s^{-1}, both very balanced, enabled the creation of the first SORFB model based on a [4]helicenium[99]. In the case of $^{nPr}DMQA^{NO2+}$, it was observed that the introduction of a nitro group on the $DMQA^+$ scaffold had consequences on the potential of the electronic processes and on the value of D, and especially of k^0. The electronic transfer in oxidation is five times less efficient in this case (k^0_{Red} = 3.7 × 10^{-2} cm·s^{-1}, k^0_{Ox} = 0.8 × 10^{-2} cm·s^{-1}), resulting in less cycling stability and robustness of the compound as published[100]. It was observed that the introduction of electron-donating groups OMe, NH_2, and NMe_2 at the X position of the $DMQA^+$ scaffold had little impact on the potential of the reduction process but contributed to a shift towards less oxidizing values of the $E_{1/2}^{Ox}$ phenomenon. This is reflected in balanced D parameters with values ranging between 4-6 × 10^{-5} cm^{-2}·s^{-1} for $^{nPr}DMQA^{NMe2+}$ and $^{nPr}DMQA^{OMe+}$, while $^{nPr}DMQA^{NH2+}$ exhibits values similar to that of the $DMQA^+$ model in correlation with low structural volume change. Similarly, for these three compounds, the k^0 values in reduction are comparable to those of $^{nPr}DMQA^+$ (~ 2 × 10^{-2} cm·s^{-1}) but two to three times higher than those in oxidation processes (≤ 1 × 10^{-2} cm·s^{-1}), an imbalance less pronounced than that of $^{nPr}DMQA^{NO2+}$. The triple Me functionalization at the Y position leading to $^{nPr}DMQA^{(pMe)3+}$ does not involve any significant changes in terms of the D parameter, with consistent values similar to those exhibited by the compounds substituted at X. However, it is noted that the k^0 in reduction appears slightly higher than that of the [4]helicenium model, whereas the k^0 of the oxidation process is more than an order of magnitude slower (k^0_{Ox} = 0.3 × 10^{-2} cm·s^{-1}), which could raise concerns about potential issues during high-rate cycling.

When the time comes to modify the R^1/R^2 arms without substituting the core, the results become significantly more pronounced. The asymmetric species, $^{n\text{Pr/Ph}}$DMQA$^+$ and $^{n\text{Pr/CH2CF3}}$DMQA$^+$, are strongly affected, with $R^2 = CH_2CF_3$ leading to a decrease of one order of magnitude in the value of *D* for the reduction process, while the oxidation process maintains a value close to that observed for the previous compounds. This disparity is also evident in k^0, with a reduction process sixteen times faster than in oxidation ($k^0_{Red} = 1.6 \times 10^{-2}$ cm·s^{-1}, $k^0_{Ox} = 0.1 \times 10^{-2}$ cm·s^{-1}); however, the fact that this phenomenon is bielectronic already eliminates this compound as a potential BRM. When $R^1 = R^2$, the *D* parameters behave more balanced, potentially related to the conservation of the molecule's symmetry. Thus, for $^{(CyNHnPr)}$DMQA$^+$, the diffusion parameters are in the range of values observed for the compounds substituted in X and Y, with an average of ~5×10^{-6} cm^2·s^{-1}. As anticipated during the CV of the compound, the $E_{1/2}^{Red}$ process is less reversible than that of its counterparts, with a value of $k^0_{Red} = 0.5 \times 10^{-2}$ cm·s^{-1}, while the oxidation maintains its reversibility. In the case of ^{PEG}DMQA$^+$, the diffusion parameters are strictly identical (6.2×10^{-6} cm^2·s^{-1}) for both electron exchanges. A noteworthy value of $k^0_{Red} = 2.5 \times 10^{-1}$ cm·s^{-1} is noted for the reduction process, which unfortunately turns out to be twenty-two times faster than the oxidative process ($k^0_{Red} = 1.1 \times 10^{-2}$ cm·s^{-1}).

As most of the ROM's electrokinetic parameters presented here fall within the range of BRMs used in reported SORFBs, this prompts us to evaluate their robustness in cycling conditions. However, deployment in a complete in-flow RFB system is a task requiring numerous specific hardware adjustments, making it unsuitable for rapid screening of new compounds. That is why we aim to emphasize the practicality and relevance of evaluating new compounds in an H-cell. This model, described as "static RFB" in the literature[37,102], has the advantage of requiring only a small volume and low working concentration while subjecting the electroactive materials to more stressful cycling constraints. This allows rapid and efficient selection and facilitates the elimination of certain candidates within an accessible timeframe.

The system used here is based on a homemade H-cell consisting of two welded glass tubes for each compartment (Figure 4A, details in Supplementary Materials) separated by a porous frit that serves as a membrane. This design is particularly suitable for BRMs as it allows us to determine whether the molecule can tolerate the use of a porous separator without ion crossover consideration. Each "pole" of the battery is equipped with a highly conductive RVC electrode that boasts a significant specific surface area (~33 cm^2 within the dimensions used in this study) and a magnetic stir bar, aiding in the diffusion of species in solution. The side where the working electrode (E_w) will be considered is also fitted with an $AgNO_3$ reference electrode, similar to the one previously employed in the characterization of a three-electrode cell.

Upon the selection of [4]helicenium exhibiting electrokinetic parameters compatible with deployment for RFB, each of them is tested at a concentration of 1 mM in acetonitrile in the presence of 0.1 M $TBAPF_6$ (0.5 M $TBABF_4$ in the case of ^{PEG}DMQA$^+$). Each side of the H-cell is filled with 5 mL of the same 1mM solution to conduct a test battery with a capacity of 134 µAh. Thus, in the initial state, each side of the static RFB contains the same BRM in the DMQA$^+$ oxidation state. During charging, an electron is transferred from the counter electrode side (E_c) to the E_w side, allowing the formation of DMQA$^{\bullet+}$ on the "posolyte" side, while the carbocation on the "negolyte" side is reduced to DMQA$^\bullet$ [Figure 4B]. The repetition of these charge-discharge cycles in our RFB model constitutes cycles.

The cycling protocol for each of the compounds involves charging and discharging at 90% of the theoretical capacity at |5| mA. Due to its static design, this type of cell primarily relies on the diffusion of species in solution to access the entirety of the electron exchange. Hence, a constant current followed by a constant voltage (CCCV) protocol was employed. This setup was developed with a reference electrode to control the

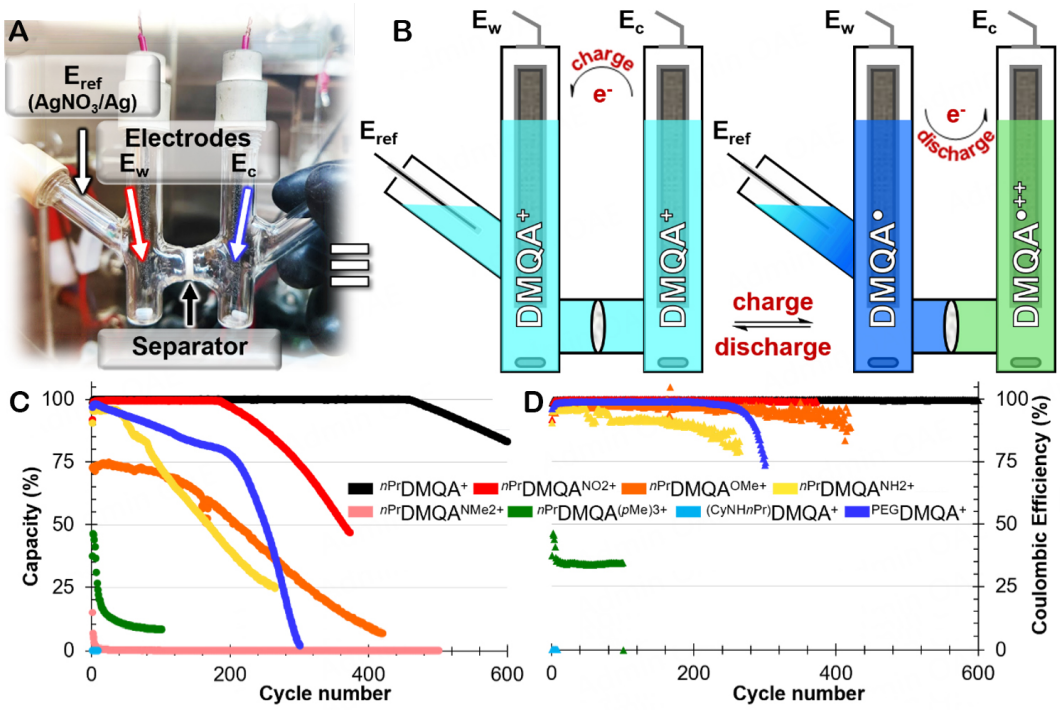

Figure 4. (A) Picture of homemade H-cell "static RFB", full details available in Supplementary Figure 9. (B) Scheme of the H-cell in initial and in charged state (reduction occurring at E_w) loaded with 2 × 5 mL of 1 mM $^{R1/R2}$DMQA$^{X/Y+}$ in 0.1 M $TBAPF_6$ CH_3CN. Display of 134 µAh H-cell cycling monitoring via (C) Capacity in discharge and (D) Coulombic efficiency of ^{nPr}DMQA$^+$, ^{nPr}DMQA^{NO2+}, ^{nPr}DMQA^{OMe+}, ^{nPr}DMQA^{NH2+}, ^{nPr}DMQA^{NMe2+}, ^{nPr}DMQA$^{(pMe)3+}$, $^{(CyNHnPr)}$DMQA$^+$ and ^{PEG}DMQA$^+$. Supplementary Figures 10-17 provide detailed monitoring of the cycling data for each helicenium individually.

voltage at Ew, and therefore, the potential limits reached will be $E_{1/2}^{Red}$ ± 300 mV. In the static RFB, the key metrics of interest are the discharge capacity (Q_{dis}) achieved and the coulombic efficiency (CE) attained during the cycles. Thus, it is observed that ^{nPr}DMQA$^+$ maintains a consistent Q_{dis} = 100% until the 461st cycle, followed by a slow degradation while maintaining a near-perfect CE (Figure 4C and D, black). Similarly, ^{nPr}DMQA^{NO2+} exhibits excellent CE, with a constant 100% Q_{dis} until the 186th cycle, after which a decrease in discharge capacity is noted until the end of cycling at the 400th cycle (Figure 4C and D, red). These findings demonstrated the relevance of this evaluation system, prompting our subsequent interest in ^{nPr}DMQA^{OMe+}. While CE is decreasing at 0.23%/cycle from an acceptable 97% value, it is noticeable that from the first cycle, the Q_{dis} is below 75% and drops rapidly at an average rate of 0.49% per cycle, making this ROM, although electrokinetically adapted, unsuitable for a SORFB system (Figure 4C and D, orange). A more surprising behavior is observed with the electron-enriched ^{nPr}DMQA^{NH2+}, with an initial Q_{dis} value of 96%, which remains stable for around forty cycles before initiating a decay at a rate of 0.28%/cycle. Meanwhile, its CE values appear slightly erratic, suggesting reactivity in the charged state, with an initial value of 96% and an average decay of 0.25%/cycle (Figure 4C and D, yellow). The transition from a primary amine to a tertiary amine for ^{nPr}DMQA^{NMe2+} has a dramatic effect on its ability to be used as a BRM. It has thus been observed that the Q_{dis}, in its case, is initially at 15%, dropping to 0% by the tenth cycle, illustrating its complete incompatibility for use in SORFB (Figure 4C and D, salmon). The introduction of three Me groups in the Y position appeared to hold promise in terms of the electrokinetic characteristics of ^{nPr}DMQA$^{(pMe)3+}$. However, when the cyclability of this new DMQA$^+$ is considered, the expected results are not met as only 46% of Q_{dis} is accessible, with an average decrease in capacity value of 0.3% per cycle. This implies that more than half of the charge has been lost between charging and discharging. This is also reflected in a CE value below 50%, which drops to 35% after ten cycles, stabilizing with a loss rate of 0.008%

per cycle (Figure 4C and D, green). Although no specific sub-species could be clearly identified, the regrettable outcome in bulk electrolysis is attributed to the intrinsic radical characteristics of the $DMQA^{\bullet+\cdot}$ and $DMQA^{\bullet}$ species. The existence of three possible benzylic radical positions, featuring heightened reactivity stemming from resonance stabilization, results in a multitude of decomposition pathways and undesired possible reactions when generated[115].

The modification of the $DMQA^{+}$ core has a significant impact on the electrophysical characteristics of ROMs, as demonstrated above. However, it seems that the variation in the nature of the R^1/R^2 arms - when allowing the conservation of two entirely reversible electrochemical events - has little effect on the electrokinetic potentials and parameters of this BRM class. However, when the cycling of $^{(CyNHnPr)}DMQA^{+}$ is assessed, the result is disastrous. The Q_{dis} is < 0.3%, and the CE value is null, illustrating how an evaluation in a three-electrode cell is insufficient for characterizing the suitability of a new BRM for SORFB. Thus, bulk electrolysis, such as static RFB cycling, is far too damaging for $^{(CyNHnPr)}DMQA^{+}$ (Figure 4C and D, cyan). Finally, the proposal to integrate pegyls arms seemed promising, as the CE value is > 98% and remains nearly constant up to cycle 200. Subsequently, a decay of 0.24% per cycle appears and can be correlated with what is observed in terms of Q_{dis} values. Indeed, it is observed that $^{PEG}DMQA^{+}$ exhibits two decay regimes: the first, from cycle 5 to 200, shows its Q_{dis} drop from 98% to 78% at a rate of 0.10% per cycle, and then, at cycle 201, this phenomenon accelerates with a decline of 0.74% per cycle (Figure 4C and D, deep blue). This behavior is not easily rationalized, but it is worth remembering that for effective discrimination, the H-cell system and the current intensities used here are extremely stressful for the electroactive material. A CE value and Q_{dis} access rates exceeding 95% still make it a convincing BRM that deserves to be evaluated in a flow system.

CONCLUSIONS

The significance of this research work resides in the practicality of an empirical methodology, selecting an ambipolar scaffold and simple electrochemistry tools, to effectively identify and screen a variety of new BRMs. The electrochemical richness of the [4]helicenium class has illustrated how the choice of a tunable core is a rapid pathway to numerous bipolar compounds with a wide range of possible substitutions. The qualification through measurements of essential electrochemical parameters, such as diffusion coefficients and electron transfer rate constants, could be carried out using a simple three-electrode cell, making this process easily accessible. Finally, the assessment of the robustness of these BRMs in a static RFB cell constitutes a quick tool for discriminating the most promising and robust ROMs in bulk electrolysis, with the future aim of deployment in a flow RFB cell. Through the importance of this research effort, we hope to assist research groups working on the development of new BRMs in accessing promising systems more swiftly.

A potential future enhancement of this methodology could involve the incorporation of Machine Learning tools capable of predicting the characteristics of potential BRMs through computational design, based on the collection of extensive data[116,117]. This would require active participation from the community in building a large database, but it has the potential to predict the entirety of electrokinetic parameters, decomposition pathways, and potential improvements for existing bipolar molecules.

DECLARATIONS

Acknowledgments

We are thankful to Mubarak Hossain and Dr. Aslam C. Shaikh for having previously synthesized batches of $^{nPr}DMQA^{+}$, $^{nPr}DMQA^{NO2+}$, $^{nPr}DMQA^{OMe+}$, $^{nPr}DMQA^{NH2+}$, and $^{nPr}DMQA^{NMe2+}$. Moutet J is grateful to Angelica P. Orlova for stimulating and inspiring discussions.

Authors' contributions

Wrote the manuscript and discussed their conclusions: Moutet J, Gianetti TL
Developed, synthetized and characterized $^{n\mathrm{Pr}}$DMQA$^{(p\mathrm{Me})3+}$: El-Assaad TH
Synthetized and characterized [6]helicenium: Kaur R
Developed, synthetized and characterized $^{n\mathrm{Pr/CH_2CF_3}}$DMQA^{+}: Mills DD
Planned the experiments and conducted all electrochemical experiments; developed, synthetized and characterized $^{(\mathrm{CyNH}n\mathrm{Pr})}$DMQA^{+}: Moutet J
All authors have given approval to the final version of the manuscript.

Availability of data and materials

Nomenclature, synthesis, CVs at various scan rates, individual H-cell cycling, and additional data are available in Supplementary Materials. ^{1}H, ^{13}C and ^{19}F NMR of each new compound are available in Supplementary Figures 18-35.

Financial support and sponsorship

Financial support comes from the University of Arizona, Salt River Project (Phoenix, AZ), and Research Corporation for Science Advancement Cottrell Scholarship 2021 (Award #27536). All NMR data were collected in the NMR facility of the Department of Chemistry and Biochemistry at the University of Arizona, RRID:SCR_012716. The purchase of the Bruker NEO 500 MHz spectrometer was supported by the National Science Foundation under Grant Number 1920234 and the University of Arizona.

Conflicts of interest

All authors declared that there are no conflicts of interest.

Ethical approval and consent to participate

Not applicable.

Consent for publication

Not applicable.

REFERENCES

1. Dresselhaus MS, Thomas IL. Alternative energy technologies. *Nature* 2001;414:332-7. DOI PubMed
2. Weitemeyer S, Kleinhans D, Vogt T, Agert C. Integration of renewable energy sources in future power systems: the role of storage. *Renew Energy* 2015;75:14-20. DOI
3. Gür TM. Review of electrical energy storage technologies, materials and systems: challenges and prospects for large-scale grid storage. *Energy Environ Sci* 2018;11:2696-767. DOI
4. International Energy Agency. Net zero roadmap: a global pathway to keep the 1.5 °C goal in reach; Paris: IEA. 2023. Available from: https://www.iea.org/reports/net-zero-roadmap-a-global-pathway-to-keep-the-15-0c-goal-in-reach [Last accessed on 13 Mar 2024].
5. Hirsh HS, Li Y, Tan DHS, Zhang M, Zhao E, Meng YS. Sodium-ion batteries paving the way for grid energy storage. *Adv Energy Mater* 2020;10:2001274. DOI
6. Shang W, Yu W, Liu Y, et al. Rechargeable alkaline zinc batteries: progress and challenges. *Energy Stor Mater* 2020;31:44-57. DOI
7. Buckingham R, Asset T, Atanassov P. Aluminum-air batteries: a review of alloys, electrolytes and design. *J Power Sources* 2021;498:229762. DOI
8. Huang H, Li D, Hou L, et al. Advanced protective layer design on the surface of Mg-based metal and application in batteries: challenges and progress. *J Power Sources* 2022;542:231755. DOI
9. Goodenough JB, Whittingham MS, Yoshino A. The Nobel prize in chemistry 2019. For the development of lithium-ion batteries. 2019. Available from: https://www.nobelprize.org/prizes/chemistry/2019/ [Last accessed on 13 Mar 2024].
10. Masias A, Marcicki J, Paxton WA. Opportunities and challenges of lithium ion batteries in automotive applications. *ACS Energy Lett* 2021;6:621-30. DOI

11. Wu J, Zhou T, Zhong B, Wang Q, Liu W, Zhou H. Designing anion-derived solid electrolyte interphase in a siloxane-based electrolyte for lithium-metal batteries. *ACS Appl Mater Interfaces* 2022;14:27873-81. DOI
12. Tarascon JM, Armand M. Issues and challenges facing rechargeable lithium batteries. *Nature* 2001;414:359-67. DOI PubMed
13. Winter M, Barnett B, Xu K. Before Li ion batteries. *Chem Rev* 2018;118:11433-56. DOI PubMed
14. Yang Z, Zhang J, Kintner-Meyer MC, et al. Electrochemical energy storage for green grid. *Chem Rev* 2011;111:3577-613. DOI
15. Badwal SP, Giddey SS, Munnings C, Bhatt AI, Hollenkamp AF. Emerging electrochemical energy conversion and storage technologies. *Front Chem* 2014;2:79. DOI PubMed PMC
16. Dunn B, Kamath H, Tarascon JM. Electrical energy storage for the grid: a battery of choices. *Science* 2011;334:928-35. DOI PubMed
17. Alotto P, Guarnieri M, Moro F. Redox flow batteries for the storage of renewable energy: a review. *Renew Sustain Energy Rev* 2014;29:325-35. DOI
18. Ravikumar MK, Rathod S, Jaiswal N, Patil S, Shukla A. The renaissance in redox flow batteries. *J Solid State Electr* 2017;21:2467-88. DOI
19. Sánchez-Díez E, Ventosa E, Guarnieri M, et al. Redox flow batteries: status and perspective towards sustainable stationary energy storage. *J Power Sources* 2021;481:228804. DOI
20. Zeng YK, Zhao TS, An L, Zhou XL, Wei L. A comparative study of all-vanadium and iron-chromium redox flow batteries for large-scale energy storage. *J Power Sources* 2015;300:438-43. DOI
21. Suttil JA, Kucharyson JF, Escalante-garcia IL, et al. Metal acetylacetonate complexes for high energy density non-aqueous redox flow batteries. *J Mater Chem A* 2015;3:7929-38. DOI
22. Beh ES, De Porcellinis D, Gracia RL, Xia KT, Gordon RG, Aziz MJ. A neutral pH aqueous organic-organometallic redox flow battery with extremely high capacity retention. *ACS Energy Lett* 2017;2:639-44. DOI
23. Lourenssen K, Williams J, Ahmadpour F, Clemmer R, Tasnim S. Vanadium redox flow batteries: a comprehensive review. *J Energy Stor* 2019;25:100844. DOI
24. Park M, Beh ES, Fell EM, et al. A high voltage aqueous zinc-organic hybrid flow battery. *Adv Energy Mater* 2019;9:1900694. DOI
25. DOE office of ARPR-E. GRIDS program overview. Available from: https://arpa-e.energy.gov/sites/default/files/documents/files/GRIDS_ProgramOverview.pdf [Last accessed on 13 Mar 2024].
26. U.S. Department of Health and Human Services Public Health Service Agency for Toxic Substances and Disease Registry. Toxicological profile for vanadium. In: ATSDR's toxicological profiles; Boca Raton, FL: CRC Press. 2012. Available from: https://www.atsdr.cdc.gov/toxprofiles/tp58.pdf [Last accessed on 20 Mar 2024].
27. Wittman RM, Perry ML, Lambert TN, Chalamala BR, Preger Y. Perspective - on the need for reliability and safety studies of grid-scale aqueous batteries. *J Electrochem Soc* 2020;167:090545. DOI
28. Park M, Ryu J, Wang W, Cho J. Material design and engineering of next-generation flow-battery technologies. *Nat Rev Mater* 2017;2:16080. DOI
29. Rhodes Z, Cabrera-pardo JR, Li M, Minteer SD. Electrochemical advances in non-aqueous redox flow batteries. *Isr J Chem* 2021;61:101-12. DOI
30. Kortekaas L, Fricke S, Korshunov A, Cekic-laskovic I, Winter M, Grünebaum M. Building bridges: unifying design and development aspects for advancing non-aqueous redox-flow batteries. *Batteries* 2023;9:4. DOI
31. Winsberg J, Hagemann T, Janoschka T, Hager MD, Schubert US. Redox-flow batteries: from metals to organic redox-active materials. *Angew Chem Int Ed* 2017;56:686-711. DOI PubMed PMC
32. Kim J, Kim Y, Yoo J, Kwon G, Ko Y, Kang K. Organic batteries for a greener rechargeable world. *Nat Rev Mater* 2023;8:54-70. DOI
33. Ding Y, Zhang C, Zhang L, Zhou Y, Yu G. Molecular engineering of organic electroactive materials for redox flow batteries. *Chem Soc Rev* 2018;47:69-103. DOI PubMed
34. Shrestha A, Hendriks KH, Sigman MS, Minteer SD, Sanford MS. Realization of an asymmetric non-aqueous redox flow battery through molecular design to minimize active species crossover and decomposition. *Chemistry* 2020;26:5369-73. DOI PubMed
35. Perry ML, Saraidaridis JD, Darling RM. Crossover mitigation strategies for redox-flow batteries. *Curr Opin Electrochem* 2020;21:311-8. DOI
36. Doris SE, Ward AL, Baskin A, et al. Macromolecular design strategies for preventing active-material crossover in non-aqueous all-organic redox-flow batteries. *Angew Chem Int Ed* 2017;56:1595-9. DOI
37. Hendriks KH, Robinson SG, Braten MN, et al. High-performance oligomeric catholytes for effective macromolecular separation in nonaqueous redox flow batteries. *ACS Cent Sci* 2018;4:189-96. DOI PubMed PMC
38. Tsehaye MT, Mourouga G, Schmidt TJ, et al. Towards optimized membranes for aqueous organic redox flow batteries: correlation between membrane properties and cell performance. *Renew Sustain Energy Rev* 2023;173:113059. DOI
39. Robb BH, George TY, Davis CM, et al. Sulfonated diels-alder poly(phenylene) membrane for efficient ion-selective transport in aqueous metalorganic and organic redox flow batteries. *J Electrochem Soc* 2023;170:030515. DOI
40. Mazumder MMR, Jadhav RG, Minteer SD. Phenyl acrylate-based cross-linked anion exchange membranes for non-aqueous redox flow batteries. *ACS Mater Au* 2023;3:557-68. DOI PubMed PMC
41. Navalpotro P, Sierra N, Trujillo C, Montes I, Palma J, Marcilla R. Exploring the versatility of membrane-free battery concept using different combinations of immiscible redox electrolytes. *ACS Appl Mater Interfaces* 2018;10:41246-56. DOI PubMed

42. Potash RA, Mckone JR, Conte S, Abruña HD. On the benefits of a symmetric redox flow battery. *J Electrochem Soc* 2016;163:A338-44. DOI
43. Janoschka T, Friebe C, Hager MD, Martin N, Schubert US. An approach toward replacing vanadium: a single organic molecule for the anode and cathode of an aqueous redox-flow battery. *ChemistryOpen* 2017;6:216-20. DOI PubMed PMC
44. Chen R. Redox flow batteries: mitigating cross-contamination via bipolar redox-active materials and bipolar membranes. *Curr Opin Electrochem* 2023;37:101188. DOI
45. Li M, Case J, Minteer SD. Bipolar redox-active molecules in non-aqueous organic redox flow batteries: status and challenges. *ChemElectroChem* 2021;8:1215-32. DOI
46. Kosswattaarachchi AM, Friedman AE, Cook TR. Characterization of a BODIPY dye as an active species for redox flow batteries. *ChemSusChem* 2016;9:3317-23. DOI
47. Ma T, Pan Z, Miao L, et al. Porphyrin-based symmetric redox-flow batteries towards cold-climate energy storage. *Angew Chem* 2018;130:3212-6. DOI
48. Geysens P, Li Y, Vankelecom I, Fransaer J, Binnemans K. Highly soluble 1,4-diaminoanthraquinone derivative for nonaqueous symmetric redox flow batteries. *ACS Sustain Chem Eng* 2020;8:3832-43. DOI
49. Tracy JS, Horst ES, Roytman VA, Toste FD. Development of high-voltage bipolar redox-active organic molecules through the electronic coupling of catholyte and anolyte structures. *Chem Sci* 2022;13:10806-14. DOI PubMed PMC
50. Liu Y, Dai G, Chen Y, et al. Effective design strategy of small bipolar molecules through fused conjugation toward 2.5 V based redox flow batteries. *ACS Energy Lett* 2022;7:1274-83. DOI PubMed PMC
51. Steen JS, Nuismer JL, Eiva V, et al. Blatter radicals as bipolar materials for symmetrical redox-flow batteries. *J Am Chem Soc* 2022;144:5051-8. DOI PubMed PMC
52. Hagemann T, Winsberg J, Häupler B, et al. A bipolar nitronyl nitroxide small molecule for an all-organic symmetric redox-flow battery. *NPG Asia Mater* 2017;9:e340. DOI
53. Hwang S, Kim H, Ryu JH, Oh SM. N-ferrocenylphthalimide; A single redox couple formed by attaching a ferrocene moiety to phthalimide for non-aqueous flow batteries. *J Power Sources* 2018;395:60-5. DOI
54. Friedl J, Lebedeva MA, Porfyrakis K, Stimming U, Chamberlain TW. All-fullerene-based cells for nonaqueous redox flow batteries. *J Am Chem Soc* 2018;140:401-5. DOI PubMed
55. Hwang S, Kim H, Ryu JH, Oh SM. N-(α-ferrocenyl)ethylphthalimide as a single redox couple for non-aqueous flow batteries. *J Power Sources* 2019;421:1-5. DOI
56. Zhen Y, Zhang C, Yuan J, Zhao Y, Li Y. Ferrocene/anthraquinone based bi-redox molecule for symmetric nonaqueous redox flow battery. *J Power Sources* 2020;480:229132. DOI
57. Xu D, Zhang C, Zhen Y, Li Y. Ferrocene/phthalimide ionic bipolar redox-active molecule for symmetric nonaqueous redox flow batteries. *ACS Appl Energy Mater* 2021;4:8045-51. DOI
58. Liu B, Tang CW, Sheong FK, Jia G, Zhao T. Artificial bipolar redox-active molecule for symmetric nonaqueous redox flow batteries. *ACS Sustain Chem Eng* 2022;10:613-21. DOI
59. Nambafu GS, Delmo EP, Bin Shahid U, et al. Pyromellitic diimide based bipolar molecule for total organic symmetric redox flow battery. *Nano Energy* 2022;94:106963. DOI
60. Etkind SI, Lopez J, Zhu YG, et al. Thianthrene-based bipolar redox-active molecules toward symmetric all-organic batteries. *ACS Sustain Chem Eng* 2022;10:11739-50. DOI
61. Duan W, Vemuri RS, Milshtein JD, et al. A symmetric organic-based nonaqueous redox flow battery and its state of charge diagnostics by FTIR. *J Mater Chem A* 2016;4:5448-56. DOI
62. Charlton GD, Barbon SM, Gilroy JB, Dyker CA. A bipolar verdazyl radical for a symmetric all-organic redox flow-type battery. *J Energy Chem* 2019;34:52-6. DOI
63. Armstrong CG, Hogue RW, Toghill KE. Application of the dianion croconate violet for symmetric organic non-aqueous redox flow battery electrolytes. *J Power Sources* 2019;440:227037. DOI
64. Raihan M, Dyker CA. Ester-substituted bispyridinylidenes: double concerted two-electron bipolar molecules for symmetric organic redox flow batteries. *ACS Energy Lett* 2023;8:3314-22. DOI
65. Winsberg J, Stolze C, Muench S, Liedl F, Hager MD, Schubert US. TEMPO/phenazine combi-molecule: a redox-active material for symmetric aqueous redox-flow batteries. *ACS Energy Lett* 2016;1:976-80. DOI
66. Dmello R, Milshtein JD, Brushett FR, Smith KC. Cost-driven materials selection criteria for redox flow battery electrolytes. *J Power Sources* 2016;330:261-72. DOI
67. Sentyurin VV, Levitskiy OA, Magdesieva TV. Molecular design of ambipolar redox-active molecules II: closed-shell systems. *Curr Opin Electrochem* 2020;24:6-14. DOI
68. Sentyurin VV, Levitskiy OA, Magdesieva TV. Molecular design of ambipolar redox-active open-shell molecules: principles and implementations. *Curr Opin Electrochem* 2020;24:15-23. DOI
69. Steen JS, de Vries F, Hjelm J, Otten E. Bipolar verdazyl radicals for symmetrical batteries: properties and stability in all states of charge. *Chemphyschem* 2023;24:e202200779. DOI PubMed
70. Broere DL, Plessius R, van der Vlugt JI. New avenues for ligand-mediated processes--expanding metal reactivity by the use of redox-active catechol, o-aminophenol and o-phenylenediamine ligands. *Chem Soc Rev* 2015;44:6886-915. DOI
71. Romero NA, Nicewicz DA. Organic photoredox catalysis. *Chem Rev* 2016;116:10075-166. DOI PubMed

72. Laursen BW, Krebs FC, Nielsen MF, Bechgaard K, Christensen JB, Harrit N. 2,6,10-Tris(dialkylamino)trioxatriangulenium ions. Synthesis, structure, and properties of exceptionally stable carbenium ions. *J Am Chem Soc* 1998;120:12255-63. DOI
73. Nicolas C, Lacour J. Triazatriangulenium cations: highly stable carbocations for phase-transfer catalysis. *Org Lett* 2006;8:4343-6. DOI PubMed
74. Goodman H, Mei L, Gianetti TL. Molecular orbital insights of transition metal-stabilized carbocations. *Front Chem* 2019;7:365. DOI PubMed PMC
75. Wilkins LC, Kim Y, Litle ED, Gabbaï FP. Stabilized carbenium ions as latent, Z-type ligands. *Angew Chem Int Ed* 2019;131:18434-8. DOI PubMed
76. Mei L, Veleta JM, Bloch J, et al. Tunable carbocation-based redox active ambiphilic ligands: synthesis, coordination and characterization. *Dalton Trans* 2020;49:16095-105. DOI
77. Litle ED, Wilkins LC, Gabbaï FP. Ligand-enforced intimacy between a gold cation and a carbenium ion: impact on stability and reactivity. *Chem Sci* 2021;12:3929-36. DOI PubMed PMC
78. Karimi M, Borthakur R, Dorsey CL, Chen CH, Lajeune S, Gabbaï FP. Bifunctional carbenium dications as metal-free catalysts for the reduction of oxygen. *J Am Chem Soc* 2020;142:13651-6. DOI PubMed
79. Shaikh AC, Veleta JM, Moutet J, Gianetti TL. Trioxatriangulenium ($TOTA^+$) as a robust carbon-based Lewis acid in frustrated Lewis pair chemistry. *Chem Sci* 2021;12:4841-9. DOI PubMed PMC
80. Mei L, Veleta JM, Gianetti TL. Helical carbenium ion: a versatile organic photoredox catalyst for red-light-mediated reactions. *J Am Chem Soc* 2020;142:12056-61. DOI
81. Mei L, Gianetti T. Helical carbenium ion-based organic photoredox catalyst: a versatile and sustainable option in red-light-induced reactions. *Synlett* 2021;32:337-4. DOI
82. Mei L, Moutet J, Stull SM, Gianetti TL. Synthesis of CF_3-containing spirocyclic indolines via a red-light-mediated trifluoromethylation/dearomatization cascade. *J Org Chem* 2021;86:10640-53. DOI
83. Hossain MM, Shaikh AC, Moutet J, Gianetti TL. Photocatalytic α-arylation of cyclic ketones. *Nat Synth* 2022;1:147-57. DOI
84. Nowack MH, Moutet J, Laursen BW, Gianetti TL. Triangulenium ions: versatile organic photoredox catalysts for green-light-mediated reactions. *Synlett* 2024;35:307-12. DOI
85. Singh PP, Singh J, Srivastava V. Visible-light acridinium-based organophotoredox catalysis in late-stage synthetic applications. *RSC Adv* 2023;13:10958-86. DOI PubMed PMC
86. Žurauskas J, Boháčová S, Wu S, et al. Electron-poor acridones and acridiniums as super photooxidants in molecular photoelectrochemistry by unusual mechanisms. *Angew Chem Int Ed* 2023;62:e202307550. DOI
87. Moutet J, Nowack MH, Mills DD, Lozier DL, Laursen BW, Gianetti TL. Planar carbenium ions for robust symmetrical all organic redox flow batteries. *Mater Adv* 2023;4:4598-606. DOI
88. Bosson J, Bisballe N, Laursen BW, Lacour J. Chapter 4: cationic triarylcarbenium helicenes: synthesis, resolution, and applications. Weinheim, Germany: Wiley; 2022. pp. 127-65. DOI
89. Herse C, Bas D, Krebs FC, et al. A highly configurationally stable [4]heterohelicenium cation. *Angew Chem Int Ed* 2003;42:3162-6. DOI
90. Laleu B, Mobian P, Herse C, et al. Resolution of [4]heterohelicenium dyes with unprecedented Pummerer-like chemistry. *Angew Chem Int Ed* 2005;44:1879-83. DOI
91. Kel O, Sherin P, Mehanna N, Laleu B, Lacour J, Vauthey E. Excited-state properties of chiral [4]helicene cations. *Photochem Photobiol Sci* 2012;11:623-31. DOI PubMed
92. Bosson J, Gouin J, Lacour J. Cationic triangulenes and helicenes: synthesis, chemical stability, optical properties and extended applications of these unusual dyes. *Chem Soc Rev* 2014;43:2824-40. DOI PubMed
93. Wallabregue A, Sherin P, Guin J, Besnard C, Vauthey E, Lacour J. Modular synthesis of pH-sensitive fluorescent diaza[4]helicenes. *Eur J Org Chem* 2014;2014:6431-8. DOI
94. Delgado IH, Pascal S, Wallabregue A, et al. Functionalized cationic [4]helicenes with unique tuning of absorption, fluorescence and chiroptical properties up to the far-red range. *Chem Sci* 2016;7:4685-93. DOI PubMed PMC
95. Li H, Voci S, Wallabregue A, et al. Efficient annihilation electrochemiluminescence of cationic helicene luminophores. *ChemElectroChem* 2017;4:1750-6. DOI
96. Tarrieu R, Delgado IH, Zinna F, et al. Hybrids of cationic [4]helicene and N-heterocyclic carbene as ligands for complexes exhibiting (chir)optical properties in the far red spectral window. *Chem Commun* 2021;57:3793-6. DOI
97. Sørensen TJ, Nielsen MF, Laursen BW. Synthesis and Stability of *N*,*N*′-Dialkyl-1,13-dimethoxyquinacridinium ($DMQA^+$): a [4]helicene with multiple redox states. *ChemPlusChem* 2014;79:1030-5. DOI
98. Shaikh AC, Moutet J, Veleta JM, et al. Persistent, highly localized, and tunable [4]helicene radicals. *Chem Sci* 2020;11:11060-7. DOI PubMed PMC
99. Moutet J, Veleta JM, Gianetti TL. Symmetric, robust, and high-voltage organic redox flow battery model based on a helical carbenium ion electrolyte. *ACS Appl Energy Mater* 2021;4:9-14. DOI
100. Moutet J, Mills D, Hossain MM, Gianetti TL. Increased performance of an all-organic redox flow battery model *via* nitration of the [4]helicenium DMQA ion electrolyte. *Mater Adv* 2022;3:216-23. DOI
101. Yan Y, Robinson SG, Sigman MS, Sanford MS. Mechanism-based design of a high-potential catholyte enables a 3.2 V all-organic nonaqueous redox flow battery. *J Am Chem Soc* 2019;141:15301-6. DOI

102. Antoni PW, Bruckhoff T, Hansmann MM. Organic redox systems based on pyridinium-carbene hybrids. *J Am Chem Soc* 2019;141:9701-11. DOI PubMed
103. Mobian P, Nicolas C, Francotte E, Bürgi T, Lacour J. Synthesis, resolution, and VCD analysis of an enantiopure diazaoxatricornan derivative. *J Am Chem Soc* 2008;130:6507-14. DOI PubMed
104. Gong K, Fang Q, Gu S, Li SFY, Yan Y. Nonaqueous redox-flow batteries: organic solvents, supporting electrolytes, and redox pairs. *Energy Environ Sci* 2015;8:3515-30. DOI
105. Korshunov A, Milner MJ, Grünebaum M, Studer A, Winter M, Cekic-laskovic I. An oxo-verdazyl radical for a symmetrical non-aqueous redox flow battery. *J Mater Chem A* 2020;8:22280-91. DOI
106. Laursen BW, Sørensen TJ. Synthesis of super stable triangulenium dye. *J Org Chem* 2009;74:3183-5. DOI
107. Bisballe N, Laursen BW. What is best strategy for water soluble fluorescence dyes? A case study using long fluorescence lifetime DAOTA dyes. *Chemistry* 2020;26:15969-76. DOI PubMed
108. Moutet J, Mills DD, Lozier DL, Gianetti TL. [4]helicenium ion as bipolar redox material for symmetrical fully organic pole-less redox flow battery. *Batteries Supercaps* 2024:e202300519. DOI
109. Helicenes: synthesis, properties and applications. Crassous J, Stará IG, Starý I, editors. Weinheim, Germany: Wiley; 2022. pp. 1-542. DOI
110. Torricelli F, Bosson J, Besnard C, Chekini M, Bürgi T, Lacour J. Modular synthesis, orthogonal post-functionalization, absorption, and chiroptical properties of cationic [6]helicenes. *Angew Chem Int Ed* 2013;52:1796-800. DOI PubMed
111. Yao Y, Lei J, Shi Y, Ai F, Lu Y. Assessment methods and performance metrics for redox flow batteries. *Nat Energy* 2021;6:582-8. DOI
112. Wang H, Sayed SY, Luber EJ, et al. Redox flow batteries: how to determine electrochemical kinetic parameters. *ACS Nano* 2020;14:2575-84. DOI
113. Nicholson RS. Theory and application of cyclic voltammetry for measurement of electrode reaction kinetics. *Anal Chem* 1965;37:1351-5. DOI
114. Lavagnini I, Antiochia R, Magno F. An extended method for the practical evaluation of the standard rate constant from cyclic voltammetric data. *Electroanalysis* 2004;16:505-6. DOI
115. Cavallotti C, Derudi M, Rota R. On the mechanism of decomposition of the benzyl radical. *Proc Combust Inst* 2009;32:115-21. DOI
116. Yao Z, Lum Y, Johnston A, et al. Machine learning for a sustainable energy future. *Nat Rev Mater* 2023;8:202-15. DOI PubMed PMC
117. Ling C. A review of the recent progress in battery informatics. *NPJ Comput Mater* 2022;8:33. DOI